Atmospheric Measurement Techniques Discussions

Atmospheric column CO_2 measurement from a new automatic ground-based sun photometer in Beijing from 2010 to 2012

Z. Q. Li[1], Y. S. Xie[1,2], X. F. Gu[1], D. H. Li[1,2], K. T. Li[1,2], X. Y. Zhang[3], J. Wu[4], and W. Xiong[4]

[1]State Environmental Protection Key Laboratory of Satellite Remote Sensing, Institute of Remote Sensing Applications, Chinese Academy of Sciences, Beijing, 100101, China
[2]University of Chinese Academy of Sciences, Beijing, 100049, China
[3]National Satellite Meteorological Centre, China Meteorological Administration, Beijing, 100081, China
[4]Anhui Institute of Optics and Fine Mechanics, Chinese Academy of Sciences, Hefei, Anhui, 230031, China

Correspondence to: Y. S. Xie (xieys@irsa.ac.cn)

Full Screen / Esc

Printer-friendly Version

Interactive Discussion

Abstract

Carbon dioxide is generally regarded as the most important greenhouse gas affecting global warming. Many researches have been conducted to measure atmospheric CO$_2$ concentration, analyze CO$_2$ variation on both seasonal and interannual scales and pre-
dict future CO$_2$ tendencies. Among them, ground-based remote sensing observation of CO$_2$ is the essential approach to provide validation data for satellite observation owning to its much higher accuracy and column CO$_2$ measurement capability. Unlike the Fourier Transform Spectrometer, the sun photometer observation system introduced in this paper takes advantages of full-automation, easily portable and mobility to provide
a non-supervised automatic field operational CO$_2$ observation approach. In this study we acquired the CO$_2$ measurements from 2010 to 2012 in Beijing, translated them to cloud free data, and designed an index related to column CO$_2$ amount. The diurnal and seasonal variations of atmospheric CO$_2$ acquired by the system were also analyzed. We compared our observation with the simulation of CarbonTracker model, and good
agreements with the model suggested the long-term stability of the system and reasonability of the data processing method. The future work will focus on absolute CO$_2$ quantity retrieval and accuracy assessment of this observation system.

1 Introduction

It is commonly accepted that as the most important greenhouse gas, carbon dioxide
plays a crucial role in global warming. The level of CO$_2$ has increased from the pre-industrial global level of 280 to 379 ppmv in 2005, in particular with 1.9 ppmv yr^{-1} in the last ten years, most probably due to human activities like burning of fossil fuel and cutting down of forests (Yokota et al., 2009). Global warming undoubtedly leads to serious consequences, like global sea level rising mainly caused by the melting
icebergs in the Polar Regions, flood in coastal areas and drought in mid-latitude regions (IPCC, 2007). Quantification of the distribution and variability of global CO$_2$ will help

people make more accurate predictions of future atmospheric CO_2 concentrations and their impacts on climate change (Ohyama et al., 2009).

Satellite observation is the only approach to monitoring global greenhouse gases distribution (Yokota et al., 2009). Two important satellites were launched by ESA and Japan respectively to detect CO_2 in the atmosphere and both successfully acquired the global CO_2 distribution and variability. Scanning Imaging Absorption Spectrometer Atmospheric Chartography (SCIAMACHY) instrument that launched with ENVISAT on 1 March 2002 for the observation of atmospheric contents such as trace gases, in particular the measurements of Greenhouse gases such as CO_2 and CH_4, is a multichannel diode array satellite spectrometer covering the spectral range from 214 nm in UV to 2386 nm in SWIR band. This spectrometer measures reflected, scattered and transmitted solar irradiation at moderate spectral resolution (0.2–1.6 nm), and performs a sequence of alternating nadir and limb measurements (Buchwitz et al., 2005a, b, 2007; Houweling et al., 2005; Barkley et al., 2006a, b, 2007; Schneising et al., 2008). Greenhouse Gases Observing Satellite (GOSAT) was launched on 23 January 2009 into a sun-synchronous orbit to monitor global atmospheric levels of CO_2 from space with two sensors onboard the satellite, Thermal and Near-infrared Sensor for Carbon Observation-Fourier Transform Spectrometer (TANSO-FTS) and Cloud and Aerosol Imager (TANSO-CAI) (Yokota et al., 2004). TANSO-FTS measures the reflected SWIR light and the thermal infrared (TIR) radiation emitted from the ground and atmosphere, and TANSO-CAI can detect thick clouds and correct the aerosol effect to help CO_2 observation.

Compared to satellite measurements, the ground-based observation acquires more accurate results, thanks to: (1) the ground-based measurements are less affected by aerosols and clouds in the atmosphere, which are the main sources of uncertainties for satellite observation; (2) compared to satellite, higher intensity of incident light at entrance of the ground-based sensor helps to acquire data with higher SNR, while as for space-based measurements, duplex-attenuation and ground surface reflection make the solar irradiation weak. Besides, ground-based instrument can keep continuous

observation to acquire the CO_2 information of a whole day, instead of single data of satellite observation, thus one can realize observation of the diurnal variation of CO_2, as the analysis in Sect. 4.1. Although the sparseness of ground-based observation limits the application to detect CO_2 in the atmosphere, it is still an indispensable part
5 of global CO_2 observation system, for providing the validation data considering observation uncertainty is the critical key parameter for CO_2 measurements when used in climate studies.

Fourier Transform Spectrometer (FTS) is one of the most popular instruments for ground-based observation of atmospheric CO_2. Yang et al. (2002) and Dufour et
10 al. (2004) demonstrated that the retrieval of column-averaged CO_2 volume mixing ratios, denoted XCO_2, could get the accuracy better than 0.5 % by ground-based FTS measurements. Washenfelder et al. (2006) achieved a precision of 0.1 % for XCO_2 values obtained from ground-based measurements, and the ~ 2 % bias was corrected against aircraft in situ measurements. However, FTS system is not easy to be moved
15 because of its large size and great weight and thus only suitable for the observation at fixed site. Moreover the FTS system is very expensive and thus somewhat affected the distribution of the observation site in the world. This paper introduced a new portable sun photometer system to implement CO_2 observation at ground station, named Automatic Sun-Tracking Spectral Radiometer (ASTSR), manufactured by CIMEL Elec-
20 tronique of Paris, France. An initial retrieval of CO_2 concentrations was performed and a Difference Absorption Index (DAI) was proposed in this paper to show the relative concentration of atmospheric CO_2.

Section 2 provided a brief description of the instrument. Section 3 introduced the observation site in Beijing and then described the data processing, including cloud
25 screening, channel selection and design of DAI index to obtain the CO_2 variation tendencies. Results were shown in Sect. 4, along with analysis of daily and seasonally variation. Besides, model simulation was showed in this section to be compared with our observation. Concluding remarks were given in Sect. 5.

Atmospheric column CO_2 measurement

Z. Q. Li et al.

Title Page

Abstract	Introduction
Conclusions	References
Tables	Figures

◄◄ ►►

◄ ►

Back Close

Full Screen / Esc

Printer-friendly Version

Interactive Discussion

2 Instrumentation

CIMEL ASTSR is a portable automatic sun photometer based on measurements of extinction of direct solar radiation at around 1.57 μm with steps of 0.5–1 nm. It contains four parts: a control and recording unit (the electronic box), a two-axis motorized rotating system, an optical sensor head, and accessories like battery and rain proof sensor. The control box is used to control the whole measurement system, with a main CPU card for the control and record electronics, and an auxiliary CPU card for the sun-tracking system. The sun-tracking system carries the optical head, which can rotate around two orthogonal axes (i.e. vertical and horizontal axes), and the positions of the two axes are recorded in the electronic box. The sensor head is composed of a photometer (for measuring direct sun irradiance), a collimator (for filtering the stray lights), a control card, a four quadrant position detector (for the precise tracking of the sun), a wedged filter driven by a stepping motor (providing 14 measurements from 1566 to 1578 nm, with nearly 1 nm step, by changing the tilt angle of the filter) and a temperature sensor. In the accessories, a storage battery is used to support the electronic box and the rain proof sensor can detect precipitation and power off the whole system when rain/snow drops in automatic mode. The main structure of this instrument is similar with CIMEL Sun Photometer CE318, but with different optical head and main CPU card. ASTSR observes atmospheric CO_2 according to a certain procedure as shown in Fig. 1.

The parameters like time, latitude/longitude, and local altitude are set to find the position of the sun after the instrument being placed, i.e. to calculate the azimuth and zenith angles so that the sensor head can rotate with the mechanic arm and point to the sun. Then the four quadrant position detector tracks the sun precisely. After that measurements of the direct solar irradiance can be made with several programmable scenarios. The direct sun measurement is composed of 14 spectral bands within about 10 seconds. In practice, a sequence of three repeated direct sun measurements is made within about 30 s, creating a triplet observation combination for the purpose of

cloud detection that introduced in Sect. 3. Triplet measurements are performed from the morning to the evening, with an equal airmass interval, which is approximately 15 min during the noon and much more dense during sunrise and sunset periods. The solar irradiance attenuated in the atmosphere enters into the collimator and then goes through the filters, suffering attenuation again before detected by the light sensor. A photoelectric element transduces the radiation into voltages, i.e. the output DN values.

3   Site and data processing

3.1   The observation site

The observation site (40°00′ N, 116°23′ E) is located on the roof of a building of Institute of Remote Sensing Applications, Chinese Academy of Sciences (IRSA, CAS) at an elevation of about 59 m, between the 4th and the 5th northern ring roads of Beijing, as shown in Fig. 2 (left panel). Beijing has a population over 20 million and a vehicle fleet of more than 5 million at the end of 2011. Major sources of CO_2 in Beijing are vehicle emissions, power plants, industry, heating boilers and construction activities (Wang et al., 2010). The main land use types around this site are roads and residential areas, while Beijing Olympic Forest Park, covering 6.8 km^2 with vegetation rate of nearly 90 %, is located less than 1 km to the northeast of the site.

Besides ASTSR system, a CE318 sun-sky radiometer is also installed at the site, from which a long-time simultaneous observation of CO_2 and aerosol has been realized, as shown in Fig. 2 (right panel). It is generally recognized that aerosol radiative forcing can cool down the global temperature, while the greenhouse gases such as CO_2 significantly heat it up. The effects on climate change of greenhouse gases have been researched a lot and several good research results have been achieved. But aerosols have many physico-chemical variations that make them versatile in the atmosphere, thus it is difficult to quantitatively estimate the cooling effect. Therefore such

Atmospheric column CO$_2$ measurement

Z. Q. Li et al.

Title Page

Abstract | Introduction

Conclusions | References

Tables | Figures

◄ | ►

◄ | ►

Back | Close

Full Screen / Esc

Printer-friendly Version

Interactive Discussion

kind of a joint observation platform is expected to provide important data to the climate change studies.

3.2 Data processing

There were 14 DNs recorded in each data record, corresponding to the 14 narrow bands from 1566 to 1578 nm. This spectral region was selected because other CO_2 absorption bands like 2.0 µm, 4.3 µm and 15 µm were often affected by other absorbers such as water vapor or easy to meet the problem of saturated absorption. However, the 1.57 µm molecular vibration absorption bands of CO_2 were relatively weak compared with other bands.

3.2.1 Cloud screening

We collected ASTSR CO_2 measurements for two years from March 2010 to March 2012. The dataset was composed of records from the sunrise to the sunset for each day, as Sect. 2 introduced. Some of the triplet observations showed significant variance because of fast moving clouds. The signal with cloud was much smaller than the normal one, even to zero if the clouds were really thick. Firstly a simple yet effective cloud detection and removal process was applied to the triplet observations. The cloud screening method was based on an assumption that during the period of a single triplet measurement (30 s) the CO_2 contents remained constant. Therefore the three measurements should be close enough to each other, ignoring small changes of the solar radiation due to sun position moves and changes of other atmospheric components like aerosols. Clouds would cause an obvious deviation among the three measurements, for the reason of its nature quick variation. We calculated the maximum, minimum and mean values of each triplet measurements, and if the three measurements were close to each other, i.e. the value of (maximum–minimum)/mean was less than a certain threshold, we considered these data as cloud free. Otherwise theses measurements were identified as contaminated by clouds. Figure 3 showed the level

1.0 (before cloud screening) data of 15 October and 29 April 2010 as an example to show the differences between cloud clear and cloud contaminated data. For CE318 observation, a triplet measurements stability test was applied that the calculated AOD should vary no more than 0.02 with in one triplet in the stable aerosol and cloud free
5 condition (Smirnov et al., 2010). To simplify the problem and exclude other interference factors, we applied the cloud screening to raw measurements. And to determine the optimal threshold for screening cloud, we set the (maximum–minimum)/mean value as 3 %, 5 % and 7 %, respectively. It was clear that the larger the threshold was the less triplet measurements would be identified as cloud free. It was significant that a balance
10 between a reasonable deviation threshold and the proportion of valid measurements should be achieved. When the threshold was less than 5 %, for example 3 %, the proportion of passed measurements of a single day significantly dropped, due to possible aerosol variations; but if the threshold was set to a large value, some thin clouds could not be detected. By comparing and analyzing the results, the threshold value was pre-
15 liminarily determined as 5 %. Figure 4 showed the measurements of 23 April 2010 before and after cloud screening by the threshold of 5 % (level 1.5) as an example. We can see from Fig. 4a that after 14:00 p.m. of the day the measurements were seriously contaminated by clouds and returned back to cloud clear after 18 o'clock in the afternoon. The cloud screening process detected and removed these contaminated triplet
20 measurements during this period, as shown in Fig. 4b.

This detection method was useful when the clouds were thin and moved fast, while maybe invalid when thick clouds blocked the solar irradiance because under that circumstance a triplet measurements would probably keep stable but with low values. These measurements could be found out by an artificial selection because these val-
25 ues were usually much smaller than normal ones. The further selection (level 2.0) was implemented to pick out and remove the abnormal measurements, including temporarily contaminated measurements by spider web. This step was rather an empirical process that should be only carefully treated by the expert. These passed measurements were then converted to hourly average values. After data pre-processing, we acquired

Title Page

Abstract | Introduction

Conclusions | References

Tables | Figures

|◀ | ▶|

◀ | ▶

Back | Close

Full Screen / Esc

Printer-friendly Version

Interactive Discussion

the data of 482 days (level 2.0), each of them contain several hourly averaged records, and these data were used for atmospheric CO_2 calculation and analysis later.

3.2.2 Channel selection and CO_2 index calculation

The irradiance attenuation could be described by CO_2 absorption depth, which can be derived from the transmittance curve around 1.57 μm region, as shown in Fig. 5. There are about ten identifiable absorption peaks from 1570 nm to 1580 nm with a moderate spectral resolution of 0.2 nm, combining two obvious absorptive features centered at 1572 nm and 1578 nm. We noticed that a very high similarity showed up between CO_2 transmittance curve and total atmosphere transmittance, as shown in Fig. 5, indicating uniform distributions of other atmospheric constituents in this region. Figure 5 also showed the 14 filter transmittance curves from 1566 nm to 1578 nm and we could see that they did not distribute as Gaussian curve strictly, and thus we convolved the filter curves to acquire equivalent center wavelengths.

We obtained the total attenuation by convolution of CO_2 transmittance with the 14 filter transmittance curves, which also helped to build up the relationship between solar irradiance and output DN values and find appropriate channels to acquire CO_2 amount. The convoluted transmittance of each band was given by:

$$T_C(i) = \int T_m(\lambda)R_i(\lambda)d\lambda \Big/ \int R_i(\lambda)d\lambda \tag{1}$$

where λ is wavelength, i is channel numbers (from 1 to 14), T_C is the convoluted transmittance, T_m denotes transmittances of atmospheric contents such as aerosol and absorbing gases, R is transmittance of the filter. The convolution transmittance was showed in Fig. 6a, along with the individual irradiation attenuation caused by water vapor, aerosol and other gases that calculated by Modtran model (Anderson et al., 1996). The transmittances of water and other gases were close to 1.00 in these channels, introducing approximately no absorption effect. The attenuation caused by aerosol was

about 0.91 but very stable for all the 14 channels, thus would not affect channel selection. According to Fig. 6a, b and US Standard Atmosphere Transmittance (1976), channel 1 (1566.71 nm) was selected as the base channel, considering that CO_2 attenuation was the weakest among the 14 channels; Next, channel 13 (1577.16 nm) was selected to represent the CO_2 absorption feature, considering: (1) to reduce the impacts of aerosols, large CO_2 absorption depth was necessary that voted channel 6 (1570.97 nm), channel 9 (1573.56 nm) and channel 13 (1577.16 nm); (2) compared with the other two channels, channel 13 was far from the base channel and thus keeping a relatively good independence, with less impacts of other channels; (3) individual calculations with these three channels were performed respectively and then compared, and it was shown that the 1577.16 nm channel was least affected by systematic noise.

Based on above analysis, a Difference Absorption Index (DAI) was proposed to represent the column CO_2 amount.

$$DAI = (DN_{base} - DN_{absorption})/(DN_{base}) \tag{2}$$

where DAI indicates the relative depth of the CO_2 absorption; DN is the instrument measurements and base and absorption denote CO_2 absorption base and the absorption feature channel, respectively (here base is channel 1, and absorption is channel 13).

As the differential absorption index was only sensitive to the relative depth of the absorption lines, there was no need for an absolute calibration of the measurement (Dufour et al., 2004). Therefore, the DAI can reflect atmospheric CO_2 contents in a relative way.

4   Results and analysis

4.1 CO_2 diurnal variations

The averaged diurnal CO_2 variations of different seasons in 2010–2012 derived from the ASTSR measurements in Beijing are shown in Fig. 7. It is clearly that the curves of four seasons have the same variation tendency without intersection. Since the instrument tracked the sun and measured the solar irradiance, there were more data records in warm seasons because of longer sunlight duration. The measurements started at about 06:00 a.m. in spring and summer, while 07:00 a.m. in autumn and 08:00 a.m. in winter; the similar time differences were revealed at the end of a day as well. The atmospheric CO_2 contents varied in the day scale with a significant factor of photosynthesis and respiration in the terrestrial ecosystem (in non-growing season some evergreen plants in Beijing still absorbed CO_2, resulting in the similar diurnal variation of CO_2 in winter). In the morning, the CO_2 DAI was at a relatively high level because the sunlight was still weak and so was the vegetation photosynthesis intensity. And it began to decrease rapidly until 10:00 to 11:00 a.m., because the CO_2 accumulated during the night before decreased fast due to increased air turbulence and consumed by strengthened photosynthesis (Pan et al., 2011). After that the reduction speed of CO_2 was slow down, and DAI reached to the lowest point around 12 o'clock in the midday, when the photosynthesis efficiency and the rate of CO_2 consumption by vegetation were the largest of a day. After that, the DAI became larger gradually in the afternoon from about 14:00 p.m. and then changed in a rapid growth for the next few hours, finally reached to the similar level in the evening as it at 06:00 or 07:00 a.m. in the morning.

These curves showed a nearly minimum-symmetrical tendency, due to solar intensity variation during the day time. From Fig. 7 we noticed that for spring, summer and autumn, DAI values at sunrise (06:00 or 07:00 a.m.) were a little higher than those at sunset (06:00 or 07:00 p.m.). This is probably because during the night the CO_2 contents were primarily controlled by respiration of vegetation, when there was no photosynthesis, i.e. no consumption of CO_2. The atmospheric CO_2 contents increased a bit

in the morning after the accumulation for a whole night. Vehicle emissions of carbon dioxide in the evening peak periods were also attributed to the difference because unlike the vehicle emissions during the morning peak, these CO$_2$ could not be absorbed by vegetation very soon. For the winter curve, DAI value in the morning was contrarily lower than the dusk DAI. This reversed relationship could be attributed to two reasons: (1) biologic respiration was weakest in winter; (2) the anthropogenic CO$_2$ emission intensity in this period was much higher than in other seasons, especially the heat supply in Northern China from late November to next March.

As can be seen in Fig. 7, the lowest points of DAI in diurnal variation were not at the same period of a day for different seasons. The maximum of CO$_2$ absorption appeared at around 13:00 p.m. in winter, at 12 o'clock in spring and autumn, and at 11:00 a.m. in summer. That was probably because the solar intensity reached to the highest level at around 12 o'clock in the mid-day for spring and autumn, and couple of minutes later for winter. The reason why it was earlier for summer was that the sunlight at 12:00 was too strong for vegetation; plants had to close their air holes in the leaves in order to weaken the transpiration and save moisture, reducing the CO$_2$ absorption.

4.2 CO$_2$ seasonal variations and comparison with the simulation

The measurements from 26 March 2010 to the same date in 2012 were used in this paper to acquire and analyze the seasonal cycle of atmospheric CO$_2$. In the total 546 measurements 482 daily averaged DAI values were calculated following the data pre-processing as introduced in Sect. 3.2.1. Figure 8 showed the CO$_2$ seasonal variations in 2010–2012 period. In the middle spring (from March to May in North China), the DAI values were at an average level about 0.115. And then CO$_2$ decreased in growing season (June to August) and got to the lowest at mid July, when the late summer of Northern China arrived with maximum vegetation coverage and plenty of CO$_2$ were absorbed by vegetation. After that vegetation started to fade away and CO$_2$ accordingly began to increase at a rapid rate, to the highest peak at mid January of the next year. City heating consuming was probably another significant cause of fast growth of

CO$_2$ since November, when the heat supply began in Beijing. For the last quarter of a "season year" (March the beginning and the next February the end) cycle, atmospheric CO$_2$ gradually decreased to the average level (but a little higher due to the CO$_2$ annual increase), with the start of vegetation growth of the next year.

The variation of atmospheric CO$_2$ during a whole year presented a periodic function curve approximately, which suggested that the daily DAI values varied with time in a sine function way. The variation tendency might be in accordance with nature because of its periodicity and symmetry. This phenomenon could be further explained by the relationship between the extraterrestrial solar illuminance E and the day number of the year dn (Kandilli and Ulgen, 2008):

$$E = E_{SC}\left\{1 + 0.034\cos\left[\frac{2\pi}{365}(dn - 2)\right]\right\} \tag{3}$$

where E_{SC} denotes the solar constant. The equation established a sine-like relation between solar illuminance and day number. We know that in most cases the photosynthetic rate increases with solar light, and more CO$_2$ are absorbed when the photosynthetic intensity is strengthened. Consequently CO$_2$ absorptive amounts are believed to have sine-like relation with time as well. Therefore the sine-like tendency of observed CO$_2$ demonstrated that vegetation photosynthesis was the dominant driving force of CO$_2$ variation at seasonal time scale.

To validate our results, CarbonTracker (Peters et al., 2007) simulation was used in this study. CarbonTracker is a system that calculates carbon dioxide uptake and release at the Earth's surface over time. Since CO$_2$ mole fractions in the atmosphere reflect the sum of all the CO$_2$ exchange at the surface, they form the combined human and natural influence on greenhouse gas levels (Tutorial-CarbonTracker2011). CO$_2$ total amount in CarbonTracker equals to the initial condition total CO$_2$, added up with the CO$_2$ due to terrestrial biosphere exchange with atmosphere (excluding wildfires), due to wildfire emissions, due to fossil fuel emissions and due to air-sea exchange. The CarbonTracker simulation uses a 34-layer model with the resolution of $3° \times 2°$ to

Z. Q. Li et al.

Full Screen / Esc

Printer-friendly Version

Interactive Discussion

calculate carbon dioxide at each layer all over the world (without North America). The dataset has four dimensions: longitude (from −180° to 180°, divided into 120 grids), latitude (from −90° to 90°, divided into 90 grids), layer (34 layers) and time (3-h averaged in a day). We calculated the daily averaged simulated CO$_2$ total amount of all

5 the 34 layers around our site from 2008 to 2010 by bi-linear interpolation, as shown in Fig. 9, since ASTSR measured the column attenuation of solar irradiance. To compare the CO$_2$ observation with the simulation, the consistency and synchronization on time should be kept but not optimized in our experiments because the CarbonTracker data were only up to the end of 2010 while the observation began at March 2010. However,

10 it also demonstrated clearly the sine-like fluctuation tendency of atmospheric CO$_2$ in the season scale as observed from our measurements. Compared the seasonal variation tendency of CO$_2$ measurements with CO$_2$ simulations from Figs. 8 and 9, both of which showed or partly showed sinusoidal variation, the differences mainly lied in two aspects: the time when CO$_2$ reached to the highest or lowest peaks and the growth

15 of atmospheric CO$_2$ year to year. This might be partly explained by the large stretch forest lied near the site, which would absorb a great deal of CO$_2$ at the surface atmosphere, not only reducing the CO$_2$ growth caused by human activities in winters such as fossil emissions and making the highest peaks occurred three months earlier, but also removing the linear growth in a year scale shown in the simulation.

20 As Fig. 10 shown, a strong linear correlation existed between our observation and CarbonTracker model for the same period, certifying that the ASTSR system was capable of measuring the atmospheric column CO$_2$ variation. All CO$_2$ scatters distributed in the area that formulated by two parallel sidelines within about 1.2 ppm. The observation and simulation were significantly correlated with the correlation coefficient R^2 of

25 0.684. The relation shown in Fig. 10 could be further used to calculate XCO$_2$ in the atmosphere with our observation.

5 Summary

The atmospheric CO_2 was measured by a new ground-based sun photometer system ASTSR based on the CO_2 absorption band at 1.57 µm. The ASTSR instrument was introduced in details, including observation principle and data processing. This system can realize the full-automatic and unsupervised field observation and has been tested for CO_2 observation at IRSA site in Beijing for 2 yr. The CO_2 contents were acquired in a way by DAI index based on difference absorption principle. Before calculating DAI, we performed data preprocess for cloud screening and abnormalities removing. The cloud detection was realized by setting a threshold of 5 % to the deviation of the triplet measurements.

The CO_2 index DAI, indicating the relative depth of CO_2 absorption, was proposed to reflect CO_2 variations. It was calculated by the measurements of a base and an absorptive channel according to difference absorption principle. We analyzed the 14 channels of the instrument, compared the impacts of atmospheric components such as water vapor and aerosols, and selected channel 13 (1577.16 nm) as the absorptive channel and channel 1 (1566.71 nm) as the base channel. DAI calculation was then performed to all the quality assured measurements and the results showed that this index successfully demonstrated the ability to represent the CO_2 variation.

We analyzed both diurnal and seasonal CO_2 variation from 2010 to 2012. For the diurnal variations, it was clear that the trends in different seasons presented similar but clearly distinguishable concaved curves, lower at noon and higher in the morning and evening, which were probably driven by photosynthesis and respiration of vegetation. The lowest CO_2 DAI point of each curve in different seasons appeared at different time (the earliest one in summer and the latest one in winter) was found and attributed to solar radiation difference between seasons. From the CO_2 daily variation we realized that CO_2 contents at the sunrise hours was a litter more than the one at sunset hours, probably due to vegetation respiration at night and vehicle emissions. For winter season, the trend was not clear because of influence of the heat supply of Beijing City.

Based on the retrieved DAI the atmospheric CO_2 changed with day number in a sine-like function way in the year scale due to vegetation photosynthesis, in accordance with the solar irradiance reached to the earth. The fast growth of CO_2 in winter with the peak appeared at mid-January was attributed to withered vegetation and strengthened anthropogenic sources. To validate the measurements of ASTSR system, a model simulation of CarbonTracker was used to compare with our observation. A significant correlation was found, demonstrating the applicability of this system. The future work will focus on instrument absolute calibration, deriving the absolute CO_2 quantities (e.g. in ppmv) and estimating the accuracy by comparison with other ground-based observations such as FTS. In addition, the sine-like trends of the seasonal variations needed to be analyzed quantitatively, for the precise assessment of CO_2 seasonal variations and annual increase caused by human activities.

References

Anderson, G. P., Kneizys, F. X., Chetwynd, J. H., Rothman, L. S., Hoke, M. L., Berk, A., Bernstein, L. S., Acharya, P. K., Snell, H. E., Mlawer, E., Clough, S. A., Wang, J. X., Lee, S. C., Revercomb, H., Yokota, T., Kimball, L. M., Shettle, E. P., Abreu, L. W., and Selby, J. E. A.: Reviewing atmospheric radiative transfer modeling: New developments in high and moderate resolution FASCODE/FASE and MODTRAN, Optical Spectroscopic Techniques and Instrumentation for Atmospheric and Space Research Ii, 2830, 82–93,doi: 10.1117/12.256105, 1996.

Barkley, M. P., Monks, P. S., Frieß, U., Mittermeier, R. L., Fast, H., Körner, S., and Heimann, M.: Comparisons between SCIAMACHY atmospheric CO_2 retrieved using (FSI) WFM-DOAS to

Title Page

Abstract | Introduction

Conclusions | References

Tables | Figures

◄ | ►

◄ | ►

Back | Close

Full Screen / Esc

Printer-friendly Version

Interactive Discussion

ground based FTIR data and the TM3 chemistry transport model, Atmos. Chem. Phys., 6, 4483–4498, doi:10.5194/acp-6-4483-2006, 2006a.

Barkley, M. P., Monks, P. S., and Engelen, R. J.: Comparison of SCIAMACHY and AIRS CO_2 measurements over North America during the summer and autumn of 2003, Geophys. Res. Lett., 33, L20805, doi:10.1029/2006gl026807, 2006b.

Barkley, M. P., Monks, P. S., Hewitt, A. J., Machida, T., Desai, A., Vinnichenko, N., Nakazawa, T., Yu Arshinov, M., Fedoseev, N., and Watai, T.: Assessing the near surface sensitivity of SCIAMACHY atmospheric CO_2 retrieved using (FSI) WFM-DOAS, Atmos. Chem. Phys., 7, 3597–3619, doi:10.5194/acp-7-3597-2007, 2007.

Buchwitz, M., de Beek, R., Burrows, J. P., Bovensmann, H., Warneke, T., Notholt, J., Meirink, J. F., Goede, A. P. H., Bergamaschi, P., Körner, S., Heimann, M., and Schulz, A.: Atmospheric methane and carbon dioxide from SCIAMACHY satellite data: initial comparison with chemistry and transport models, Atmos. Chem. Phys., 5, 941–962, doi:10.5194/acp-5-941-2005, 2005a.

Buchwitz, M., de Beek, R., Noël, S., Burrows, J. P., Bovensmann, H., Bremer, H., Bergamaschi, P., Körner, S., and Heimann, M.: Carbon monoxide, methane and carbon dioxide columns retrieved from SCIAMACHY by WFM-DOAS: year 2003 initial data set, Atmos. Chem. Phys., 5, 3313–3329, doi:10.5194/acp-5-3313-2005, 2005b.

Buchwitz, M., Schneising, O., Burrows, J. P., Bovensmann, H., Reuter, M., and Notholt, J.: First direct observation of the atmospheric CO_2 year-to-year increase from space, Atmos. Chem. Phys., 7, 4249–4256, doi:10.5194/acp-7-4249-2007, 2007.

Dufour, E., Bréon, F. M., and Peylin, P.: CO_2 column averaged mixing ratio from inversion of ground-based solar spectra, J. Geophys. Res-Atmos., 109, D09304, doi:10.1029/2003jd004469, 2004.

Houweling, S., Hartmann, W., Aben, I., Schrijver, H., Skidmore, J., Roelofs, G.-J., and Breon, F.-M.: Evidence of systematic errors in SCIAMACHY-observed CO_2 due to aerosols, Atmos. Chem. Phys., 5, 3003–3013, doi:10.5194/acp-5-3003-2005, 2005.

Intergovernmental Panel on Climate Change (IPCC): Climate Change 2007: The Physical Science Basis: Contribution of Working Group I to the Fourth Assessment Report of the IPCC, Cambridge Univ. Press, New York, 2007.

Kandilli, C. and Ulgen, K: Solar illumination and estimating daylight availability of global solar irradiance, Energy Sources Part a-Recovery Utilization and Environmental Effects, 30, 1127–1140, doi:10.1080/15567030601100688, 2008.

Title Page

Abstract | Introduction

Conclusions | References

Tables | Figures

◄ | ►

◄ | ►

Back | Close

Full Screen / Esc

Printer-friendly Version

Interactive Discussion

Ohyama, H., Morino, I., Nagahama, T., Machida, T., Suto, H., Oguma, H., Sawa, Y., Matsueda, H., Sugimoto, N., Nakane, H., and Nakagawa, K.: Column-averaged volume mixing ratio of CO_2 measured with ground-based Fourier transform spectrometer at Tsukuba, J. Geophys. Res.-Atmos., 114, D18303, doi:10.1029/2008jd011465, 2009.

Pan, J. B., Dong, L., Liao, S. X., Yan, H., Qiao, L., and Li, C.: CO_2 concentration characteristics in Beijing Olympic Forest Park, Journal of Beijing Forestry University, 33, 30–35, 2011.

Peters, W., Jacobson, A. R., Sweeney, C., Andrews, A. E., Conway, T. J., Masarie, K., Miller, J. B., Bruhwiler, L. M. P., Petron, G., Hirsch, A. I., Worthy, D. E. J., van der Werf, G. R., Randerson, J. T., Wennberg, P. O., Krol, M. C., and Tans, P. P.: An atmospheric perspective on North American carbon dioxide exchange: CarbonTracker, P. Natl. Acad. Sci. USA, 104, 18925–18930, 2007.

Schneising, O., Buchwitz, M., Burrows, J. P., Bovensmann, H., Reuter, M., Notholt, J., Macatangay, R., and Warneke, T.: Three years of greenhouse gas column-averaged dry air mole fractions retrieved from satellite – Part 1: Carbon dioxide, Atmos. Chem. Phys., 8, 3827–3853, doi:10.5194/acp-8-3827-2008, 2008.

Smirnov, A., Holben, B. N., Eck, T. F., Dubovik, O., and Slutsker, I.: Cloud-screening and quality control algorithms for the AERONET database, Remote. Sens. Environ., 73, 337–349, 2000.

Tutorial-CarbonTracker2011: http://www.esrl.noaa.gov/gmd/ccgg/carbontracker/tutorial.html/, last access: 15 August 2012.

Wang, Y., Munger, J. W., Xu, S., McElroy, M. B., Hao, J., Nielsen, C. P., and Ma, H.: CO_2 and its correlation with CO at a rural site near Beijing: implications for combustion efficiency in China, Atmos. Chem. Phys., 10, 8881–8897, doi:10.5194/acp-10-8881-2010, 2010.

Washenfelder, R. A., Toon, G. C., Blavier, J. F., Yang, Z., Allen, N. T., Wennberg, P. O., Vay, S. A., Matross, D. M., and Daube, B. C.: Carbon dioxide column abundances at the Wisconsin Tall Tower site, J. Geophys. Res-Atmos., 111, D22305, doi:10.1029/2006jd007154, 2006.

Yang, Z. H., Toon, G. C., Margolis, J. S., and Wennberg, P. O.: Atmospheric CO2 retrieved from ground-based near IR solar spectra, Geophys. Res. Lett., 29, 1339, doi:10.1029/2001gl014537, 2002.

Yokota, T., Oguma, H., Morino, I., Higurashi, A., Aoki, T., and Inoue, G.: Test measurements by a BBM of the nadir-looking SWIR FTS aboard GOSAT to monitor CO_2 column density from space, Passive Optical Remote Sensing of the Atmosphere and Clouds Iv, 5652, 182–188, 2004.

Title Page

Abstract | Introduction

Conclusions | References

Tables | Figures

|◀ | ▶|

◀ | ▶

Back | Close

Full Screen / Esc

Printer-friendly Version

Interactive Discussion

Yokota, T., Yoshida, Y., Eguchi, N., Ota, Y., Tanaka, T., Watanabe, H., and Marksyutov, S.: Global concentrations of CO_2 and CH_4 retrieved from GOSAT: First preliminary results, Scientific Online Letters on the Atmosphere, 5, 160–163, 2009.

Title Page

Abstract | Introduction

Conclusions | References

Tables | Figures

◄ | ►

◄ | ►

Back | Close

Full Screen / Esc

Printer-friendly Version

Interactive Discussion

Discussion Paper | Discussion Paper | Discussion Paper | Discussion Paper
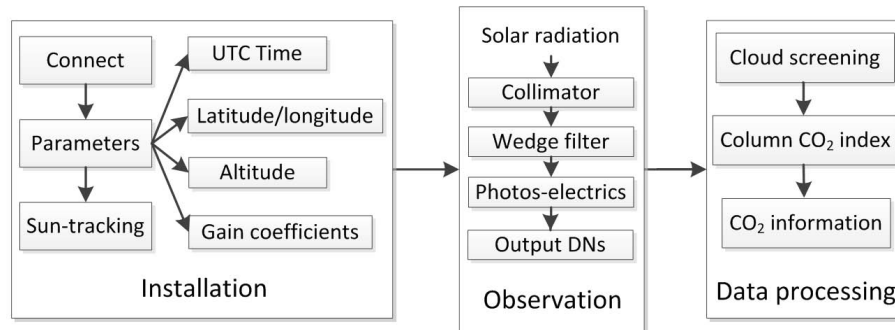
Fig. 1. The observation process of ground-based CO$_2$ sun photometer, from instrument installation to data processing.

Z. Q. Li et al.
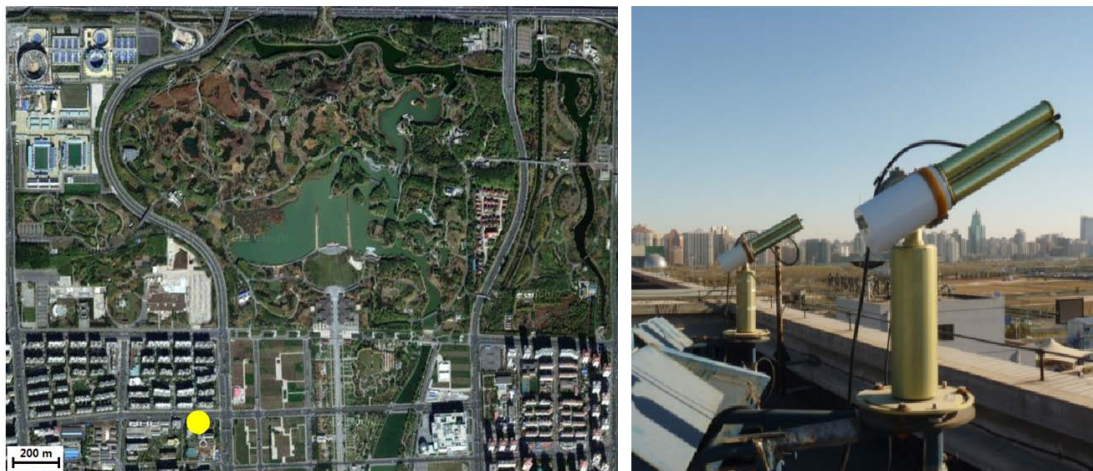
Fig. 2. The left panel shows IRSA site location in the region. The yellow solid circle in the lower left corner of the panel denotes IRSA site, where the Olympic Forest Park (the large dark green region) lies nearby. The right panel shows the Simultaneous Observation Platform of CO$_2$ and aerosol at IRSA site, with the CO$_2$ photometer on the right and the Aerosol photometer (CE318) on the left.
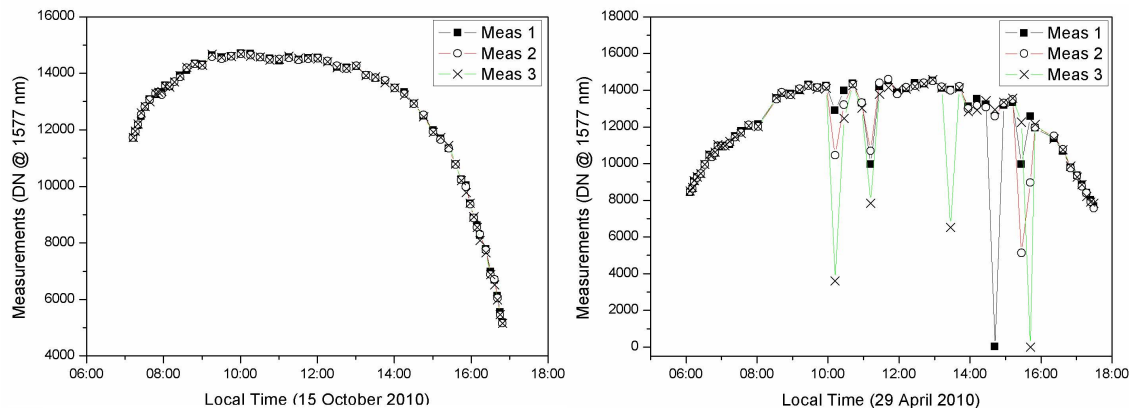
Fig. 3. Original triplet measurements (level 1.0, 1577 nm) on 15 October and 29 April 2010. On the left panel three sets of measurements are close to each other indicating cloud free condition. The right panel shows significant differences between the three sets of measurements, indicating cloud contamination.
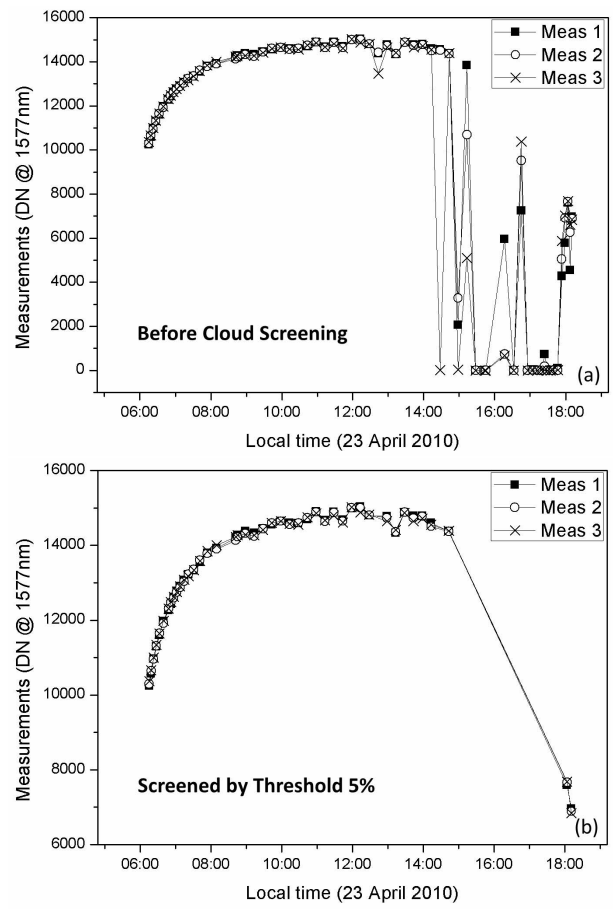
Fig. 4. Cloud detection and removal process based on the triplet measurements of 23 April 2010, with the threshold 5 %. **(a)** The original measurements (level 1.0, 1577 nm). **(b)** Cloud contaminated measurements were screened by the threshold of 5 %.
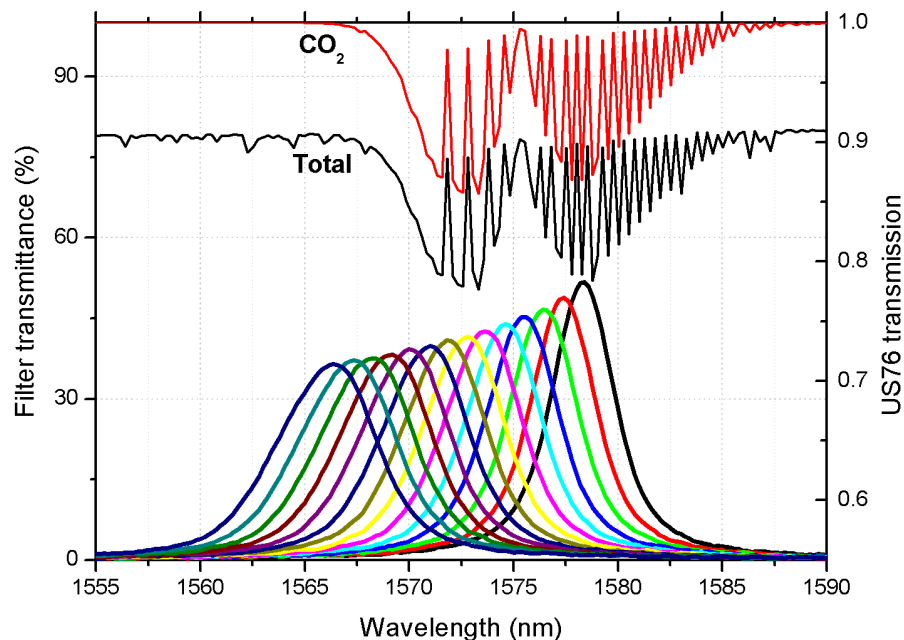
Fig. 5. The transmittance curves of CO_2 and the total atmosphere (right axis), calculated by Modtran with resolution of 0.25 nm, using US Standard Atmosphere of 1976. The 14 filter transmittance curves (centered from 1566 to 1578 nm of ASTSR) are displayed following left axis.
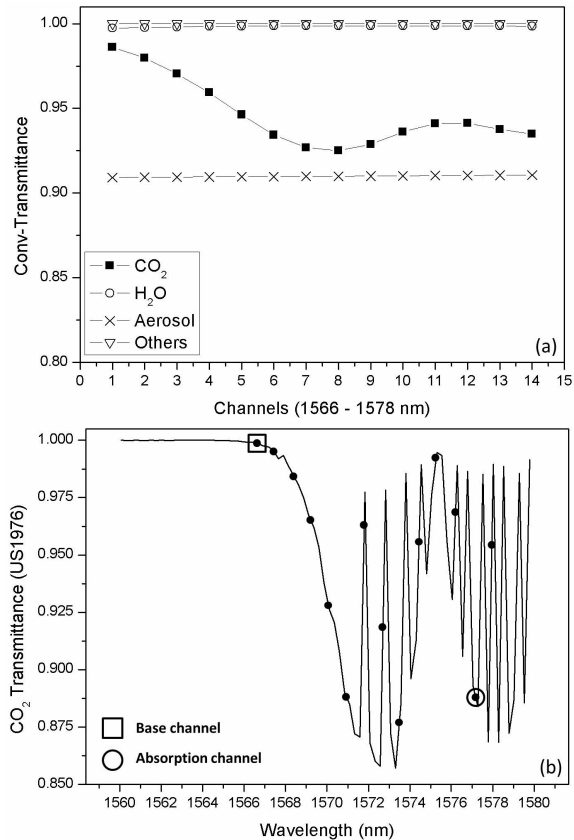
Fig. 6. (a) Convoluted transmittances of atmospheric constituents (with the transmittance of 14 filters of ASTSR). The transmittance of water vapor and other gases are very close to 1.00, causing little attenuation to the solar irradiance. **(b)** Locations of the 14 equivalent centers at CO_2 transmittance curve. The box denotes the selected base channel, and the circle denotes the selected absorption channel.
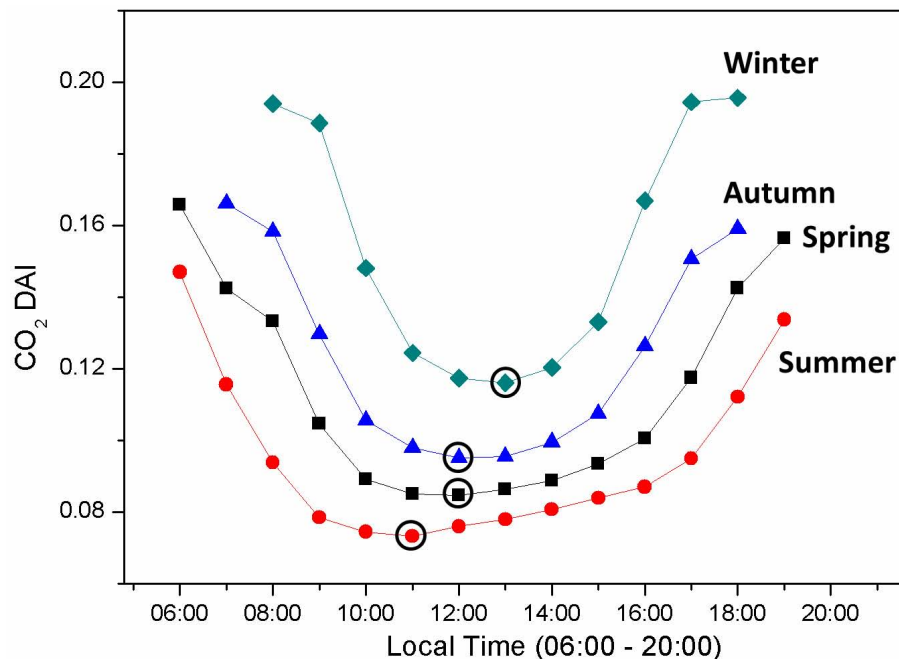
Fig. 7. Averaged CO_2 DAI at different seasons in Beijing during 2010–2012. The black circles shows the lowest DAI values (i.e. the maximum CO_2 absorption). For spring and autumn, the maximum absorption appeared at 12 o'clock in the mid-day, while at 11:00 a.m. and 13:00 p.m. for summer and winter, respectively.
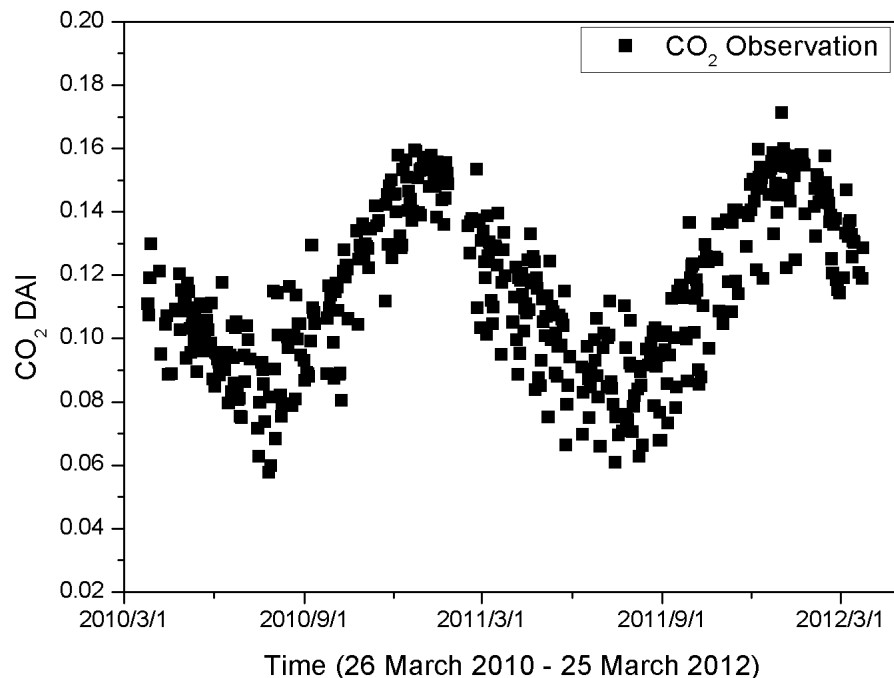
Fig. 8. The seasonal variation of CO_2 DAI in two years from 2010 to 2012, IRSA site, Beijing. The distribution of DAI scatters (daily averaged) shows a sine-like function trend, with the period cycle of about one year. The CO_2 DAI reached to the lowest level at late July, while at middle January the value of the index was the highest.

Title Page

Abstract | Introduction

Conclusions | References

Tables | Figures

◄ | ►

◄ | ►

Back | Close

Full Screen / Esc

Printer-friendly Version

Interactive Discussion
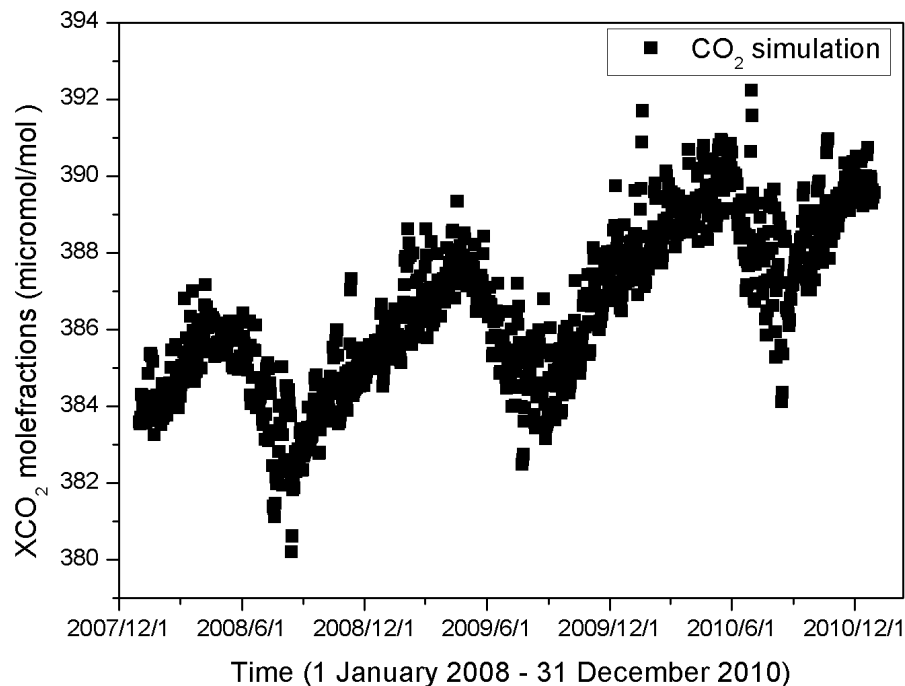
Fig. 9. The seasonal variation of CO_2 mole fractions (daily averaged) simulated by Carbon-Tracker from 2008 to 2010 at Beijing region. An interannual fluctuation of atmospheric CO_2 that presented an approximate sine function trend appeared. There was an increased year to year trend showed up as well.
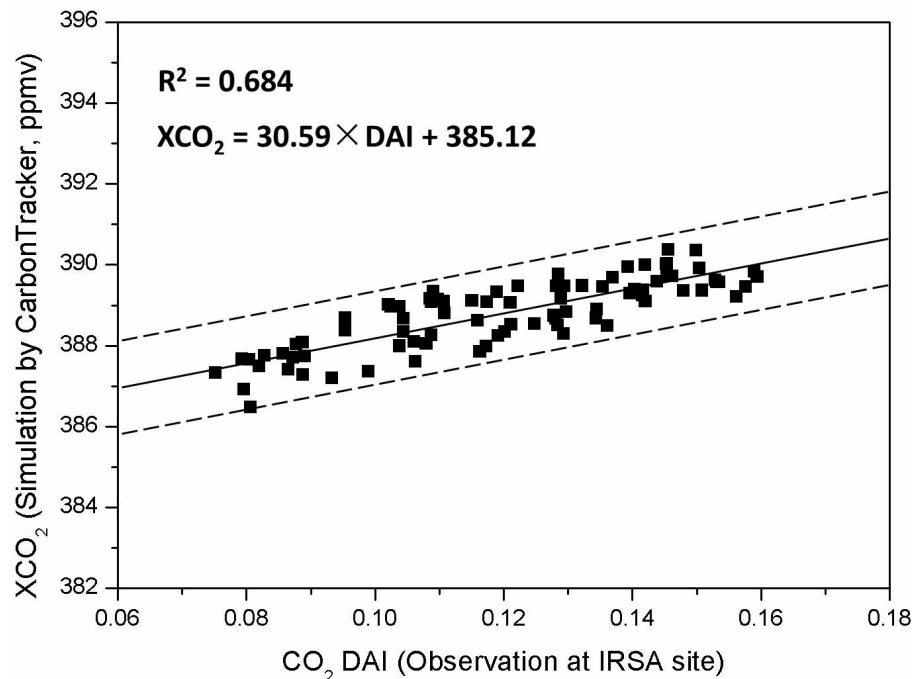
Fig. 10. The correlation plot of daily averaged CO_2 amounts between CarbonTracker model and the observation at IRSA site for the same period (March to December in 2010). The solid line denotes the linear fitting of the observed and modeled CO_2 while all of scatters distribute within the region of about ±1.2 ppm (indicated by the two dash lines).